



Citation for published version:

Pang, T, Aye Chan, TS, Jande, YAC & Shen, J 2020, 'Removal of fluoride from water using activated carbon fibres modified with zirconium by a drop-coating method', *Chemosphere*, vol. 255, 126950, pp. 126950. <https://doi.org/10.1016/j.chemosphere.2020.126950>

DOI:

[10.1016/j.chemosphere.2020.126950](https://doi.org/10.1016/j.chemosphere.2020.126950)

Publication date:

2020

Document Version

Peer reviewed version

[Link to publication](#)

Publisher Rights

CC BY-NC-ND

University of Bath

Alternative formats

If you require this document in an alternative format, please contact:
openaccess@bath.ac.uk

General rights

Copyright and moral rights for the publications made accessible in the public portal are retained by the authors and/or other copyright owners and it is a condition of accessing publications that users recognise and abide by the legal requirements associated with these rights.

Take down policy

If you believe that this document breaches copyright please contact us providing details, and we will remove access to the work immediately and investigate your claim.

1 ***Removal of fluoride from water using activated carbon fibres modified***
2 ***with zirconium by a drop-coating method***

3
4 Tianting Pang¹, Thet Su Aye Chan¹, Yusufu Abeid Chande Jande^{2,3}, Junjie Shen^{1,4,5*}

5
6 ¹Department of Chemical Engineering, University of Bath, Bath BA2 7AY, UK

7 ²Water Infrastructure and Sustainable Energy Futures (WISE-Futures) Center, Nelson
8 Mandela African Institution of Science and Technology, Arusha, Tanzania

9 ³Department of Materials and Energy Science and Engineering, Nelson Mandela African
10 Institution of Science and Technology, Arusha, Tanzania

11 ⁴Centre for Advanced Separations Engineering (CASE), University of Bath, Bath BA2
12 7AY, UK

13 ⁵Water Innovation and Research Centre (WIRC), University of Bath, Bath BA2 7AY, UK

14
15 Resubmitted to

16 *Chemosphere*

17 April 2020

18 Word count: 5251 words + 4 figures

19
20 *Corresponding author: J.Shen@bath.ac.uk

21 **Abstract:**

22 Metal-modified carbon materials have been widely used for fluoride removal, but the
23 traditional impregnation by soaking method suffers from low loading of metals and substantial
24 use of chemicals. This study proposed a new approach to prepare zirconium modified activated
25 carbon fibres (Zr-ACF) by a drop-coating method. Using the same amount of chemicals, the
26 drop-coating method yielded a 5.5 times higher fluoride adsorption capacity than the soaking
27 method due to more effective loading of Zr(IV) onto ACF. The effects of various preparation
28 conditions, including the addition of a complexing agent (oxalic acid) and Zr/ACF mass ratio (0-
29 1), were investigated. Zr-ACF prepared by drop-coating was characterised by SEM and BET,
30 and the functional groups involved in the anchoring of Zr(IV) on ACF and the adsorption of
31 fluoride onto Zr-ACF were identified by FTIR and XPS. Adsorption experiments at pH between
32 3 and 11 revealed that ion exchange and electrostatic attraction were the main adsorption
33 mechanisms at different pH levels. Co-existing anions such as CO_3^{2-} , HCO_3^- and Cl^- had an
34 insignificant negative impact (<5%) on fluoride adsorption capacity while SO_4^{2-} decreased
35 fluoride adsorption capacity by 11.5%. The adsorption kinetics followed the pseudo-second-
36 order model. The adsorption isotherms followed the Langmuir isotherm model with a maximum
37 fluoride adsorption capacity of 28.50 mg/L at 25 °C, which was higher than other carbon-based
38 materials in the literature. The remarkable improvement of adsorption capacity and reduced
39 chemical consumption demonstrate that Zr-ACF prepared by drop-coating is a promising
40 adsorbent for fluoride removal.

41

42 **Keywords:**

43 Drop-coating; activated carbon fibre; zirconium; fluoride; adsorption

44 **1. Introduction**

45 Fluorine is abundant in the natural environment and can be accumulated in the human
46 body via food and water (Akuno et al., 2019). A low concentration of fluoride in water (< 1
47 mg/L) is beneficial for preventing dental caries and tooth decay (Petersen and Ogawa, 2016).
48 Conversely, long-time ingestion of high concentrations of fluoride causes many health problems
49 such as dental and skeletal fluorosis (Ali et al., 2016), lower intelligence of children (Green et al.,
50 2019) and bone cancer (Crnosija et al., 2019). The World Health Organization (WHO)
51 recommends a fluoride guideline value in drinking water of 1.5 mg/L (World Health
52 Organization, 2017). Globally, more than 200 million people suffer from excess fluoride in
53 drinking water, particularly in developing countries such as Kenya (Malago et al., 2017),
54 Tanzania (Fawell et al., 2006), India (Mukherjee and Singh, 2018; Ali et al., 2019), Iran (Amini
55 et al., 2016; Dehghani et al., 2019; Yousefi et al., 2019) and China (Wang et al., 2019; Zhang et
56 al., 2020).

57 Adsorption is one of the most used methods for defluoridation due to its simple operation,
58 low energy consumption, and low cost, compared with other methods such as ion exchange
59 (Sundaram and Meenakshi, 2009), coagulation (He et al., 2016; Gan et al., 2019), flocculation
60 (Wang et al., 2013), precipitation (Lu and Liu, 2010), reverse osmosis (Shen and Schäfer, 2015;
61 Owusu-Agyeman et al., 2019) and electrodialysis (Grzegorzec and Majewska-Nowak, 2016).
62 Carbon-based adsorbents with high surface area and low-cost precursor sources, including
63 activated carbon (Talat et al., 2018), carbon nanotubes (Ansari et al., 2011), and activated carbon

64 fibre (ACF) (Bhaumik and Mondal, 2015), have attracted great attention in recent years. But the
65 physical interactions between these carbon adsorbents and fluoride are still weak which restricts
66 their adsorption capacity. Metal oxides and hydroxides have been used to modify carbon
67 adsorbents, which can not only increase surface area but also enhance the interactions with
68 fluoride. Successful examples include lanthanum (La) modified granular activated carbon (GAC)
69 (Vences-Alvarez et al., 2015), zirconium (Zr) modified GAC (Velazquez-Jimenez et al., 2013),
70 Zr modified powdered activated carbon (PAC) (Mullick and Neogi, 2018), aluminium (Al) and
71 cerium (Ce) modified GAC (Kalidindi et al., 2016), and titanium (Ti) modified PAC (Li et al.,
72 2018).

73 Impregnation by soaking is a well-established method to modify the carbon-based
74 adsorbents. After impregnation by soaking, the specific surface area of adsorbents can increase
75 up to 10 times (García-Sánchez et al., 2016) and their defluoridation capacities also rise
76 (Daifullah et al., 2007; Nie et al., 2012). However, the amount of metal oxides and hydroxides
77 used in the soaking method is far more than what is required, which may lead to the formation of
78 metallic crystals that are unevenly distributed in the pores and cause channel blockage
79 (Velazquez-Jimenez et al., 2013). This is why the adsorption capacity is not proportional to the
80 amount of metal used, especially in a high concentration soaking solution. To solve this problem,
81 researchers proposed to use complexing agents such as oxalic acid, citric acid, and malic acid
82 (Wang et al., 2011; Velazquez-Jimenez et al., 2013) to improve metal dispersion and control the
83 growth of nucleation. But such extra consumption of chemicals results in significant waste and is
84 against the goal of Green Chemistry.

85 Drop-coating is another impregnation method which applies a thin layer of a solution
86 dropwise to the surface of the sample and allows it to evaporate. To achieve the same level of

87 impregnation, the drop-coating method consumes much fewer chemicals and water than the
88 soaking method, thus having a lower process mass intensity (PMI) (Welton, 2015). In recent
89 years, this method has been successfully applied in acoustic chemical sensor arrays (Li, 2011)
90 and enhanced Raman spectroscopy (Halvorson et al., 2011).

91 This research adopted the drop-coating method to modify ACF with Zr. ACF was
92 preferably used over other carbon-based materials because of its larger surface area, more
93 uniform micropore size distribution and fabric form for ease of handling (Saha and Grappe,
94 2017). Zr was chosen due to its strong and selective affinity towards fluoride (Górski et al.,
95 2005). Various preparation parameters including the addition of complexing agents and Zr/ACF
96 mass ratio were optimized. Zr-ACF was systematically characterised by SEM, BET, FTIR and
97 XPS. The effects of solution pH and co-existing anions on the defluoridation process were
98 researched and the possible fluoride adsorption mechanisms were proposed. Adsorption kinetics,
99 isotherms, and thermodynamics were also studied.

100

101 **2. Materials and methods**

102 *2.1. Materials and chemicals*

103 The commercial knitted ACF, FLEXZORB FM50K, was obtained from Chemviron
104 Carbon Cloth Division, UK. Zirconium(IV) dichloride oxide octahydrate ($\text{ZrOCl}_2 \cdot 8\text{H}_2\text{O}$), oxalic
105 acid (OA), sodium fluoride (NaF), sodium chloride (NaCl), sodium bicarbonate (NaHCO_3),
106 sodium carbonate (Na_2CO_3), sodium sulphate (Na_2SO_4), potassium chloride (KCl), sodium
107 hydroxide (NaOH), hydrochloric acid (HCl), and nitric acid (HNO_3) were purchased from Fisher

108 Scientific, UK. All the chemicals were of analytical grade. Deionized (DI) water was produced
109 by PURELAB Chorus, ELGA, UK.

110 *2.2. Preparation of adsorbents*

111 **Pre-treatment.** The as-received ACF was cleaned with 5 M HNO₃ and was repeatedly
112 rinsed with DI water until the pH of the washing liquid was close to 7. Afterwards, ACF was
113 dried in an oven at 105 °C for 12 h before use.

114 **Impregnation.** The Zr-ACF adsorbents were prepared by two wet impregnation methods,
115 namely soaking and drop-coating. The soaking method was modified from a previous study
116 which used OA as the complexing agent (Velazquez-Jimenez et al., 2013). Briefly, 0.1 g of ACF
117 was sheared to the desired size fragment (0.4-0.6 cm) and was soaked into 10 mL of Zr(IV)
118 solution (Zr/ACF mass ratio = 1). The Zr-ACF suspension was stirred for 1 h and then was
119 mixed with 10 mL of OA solution (Zr/OA mass ratio = 1.5) and stirred for another 1 h. The solid
120 Zr-ACF was collected by filtration, washed with DI water, and dried at 105 °C for 12 h. For
121 comparison purposes, Zr-ACF that did not contain OA was prepared by soaking 0.1 g of ACF
122 into 20 mL of Zr(IV) solution (Zr/ACF mass ratio = 1) for 2 h.

123 The drop-coating method used Zr(IV) solutions with a much smaller volume. Briefly, 0.1
124 g of ACF was uniformly drop-coated with 2 mL of Zr(IV) solution (Zr/ACF mass ratio = 0.2-1)
125 and was dried in the oven at 105 °C for 12 h. Subsequently, Zr-ACF was drop-coated with 4 mL
126 of OA solution (Zr/OA mass ratio = 1.5) and was dried again in the oven at 105 °C for 12 h. For
127 comparison purposes, Zr-ACF that did not contain OA was prepared by drop-coating 0.1 g of
128 ACF with 2 mL of Zr(IV) solution (Zr/ACF mass ratio = 0.2-1). To ensure that the impregnated

129 Zr(IV) does not leak from Zr-ACF, some Zr-ACF samples were washed with DI water after
130 drying and their adsorption capacities were compared to the unwashed Zr-ACF.

131 ***2.3. Characterization techniques***

132 The surface morphology of ACF and Zr-ACF was observed by a scanning electron
133 microscope (SEM) (JSM-6480LV, JEOL, Japan). Nitrogen adsorption-desorption isotherms
134 were performed at 77 K using a 3Flex Surface Characterization Analyzer (Micromeritics, USA).
135 The specific surface area was calculated from the BET theory and the pore size distribution and
136 pore volume were calculated using the Horvath-Kawazoe model. Fourier-transform infrared
137 spectroscopy (FTIR) analysis was conducted using a Frontier FTIR spectrometer (PerkinElmer,
138 USA) with KBr pellets. The FTIR spectra were recorded with 32 scans at a resolution of 4 cm⁻¹.
139 X-ray photoelectron spectroscopy (XPS) measurements were performed by an AXIS Ultra DLD
140 system (Kratos, UK) using monochromatic Al K α X-ray source operating at 120 W. XPS data
141 were analysed using CasaXPS (v2.3.19 rev 1.11) after subtraction of a Shirley background. The
142 pH value at the point of zero charge (pH_{PZC}) was determined by the batch equilibration technique
143 (Shen et al., 2018). A solution of 0.1 M KCl was prepared and its initial pH was adjusted
144 between 3 and 11 by using 0.1 M HCl/NaOH solution. 200 mg of Zr-ACF was added to 100 mL
145 of KCl solution and the suspension was stirred at 298 K for 24 h until the pH stabilized. The final
146 pH was measured and the difference between initial and final pH (pH_{initial}-pH_{final}) was plotted
147 against the initial pH. The pH_{PZC} was obtained from the intersection point of the plot. The
148 speciation of fluoride in NaF solution was calculated by using Visual MINTEQ version 3.1
149 (KTH, Sweden).

150 **2.4. Adsorption experiments**

151 The adsorption of fluoride onto Zr-ACF was carried out in batch adsorption experiments.
152 Fluoride stock solution of 200 mg/L was prepared by dissolving 0.221g of NaF in 500 mL of DI
153 water. Other fluoride solutions were made by subsequent dilutions of the stock solution. A fixed
154 Zr-ACF dose of 2 g/L was used in all experiments.

155 In a typical adsorption experiment, 200 mg of Zr-ACF was added to 100 mL of 20 mg/L
156 fluoride solution and stirred on the hotplate at 400 rpm and 25 °C. At regular intervals, 5 mL of
157 the suspension was withdrawn and centrifugated by a benchtop centrifuge (Medifuge, Thermo
158 Scientific, UK). The fluoride concentration in the supernatant was determined by a pH/ion meter
159 coupled with a fluoride ion-selective electrode (S220 and perfectION, Mettler Toledo, USA).
160 Before measurement, the sample was mixed with an equal volume of the total ionic strength
161 adjustment buffer (TISAB II) solution to minimize the effects of complexions and solution pH.
162 The adsorption capacity of Zr-ACF (q_t , mg/g) was calculated from Equation (1) (Dehghani et al.,
163 2017):

$$165 \quad q_t = \frac{(C_0 - C_t)V}{m} \quad (1)$$

166
167 where C_0 and C_t are the initial and present fluoride concentrations (mg/L), V is the volume of the
168 solution (mL), and m is the mass of the adsorbent used (g).

169 To investigate the effect of solution pH on adsorption capacity, the initial pH of the
170 fluoride solution was adjusted from 3 to 11 (increment by 2) by using 1 mM HCl or 1 mM
171 NaOH solution. The final pH after fluoride adsorption was also measured. To study the effect of

172 co-existing anions, solutions containing 20 mg/L of fluoride and 20 mg/L of another anion
173 (chloride, bicarbonate, carbonate, and sulphate) were prepared. The methods and equations to
174 determine the adsorption kinetics, isotherms and thermodynamics were included in the
175 Supplementary Information. All the experiments were done in triplicate and the average values
176 of the results were used for data analysis.

177

178 **3. Results and discussion**

179 ***3.1. Optimization of the preparation methods***

180 **3.1.1. Different impregnation methods**

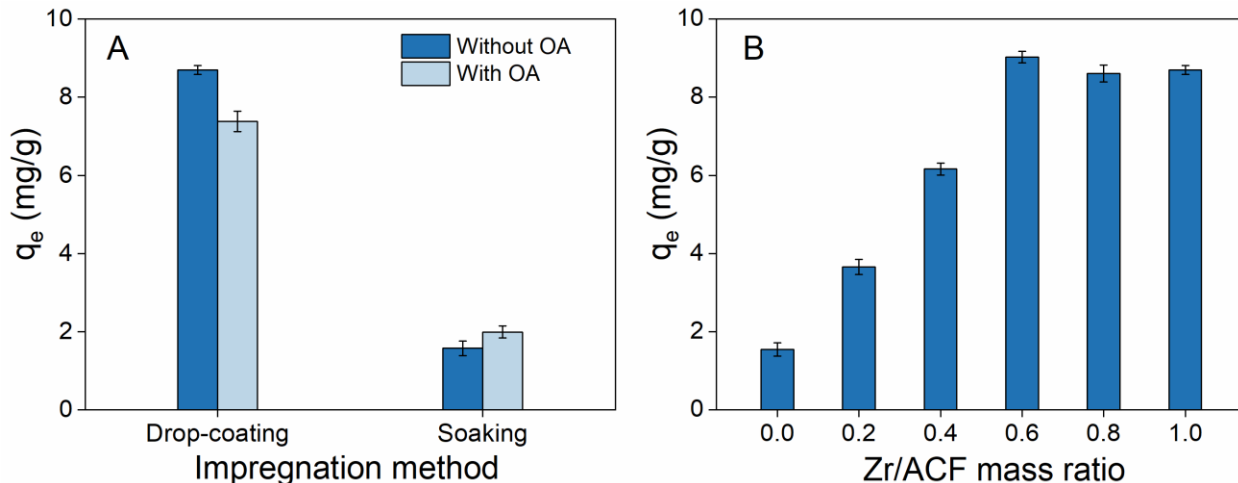
181 When comparing the effectiveness of different impregnation methods, only the adsorbents
182 with the same Zr/ACF and Zr/OA mass ratios were used. The fluoride adsorption capacities of
183 Zr-ACF prepared by different impregnation methods are shown in Figure 1(A). It can be seen
184 that the drop-coating method yielded a q_e of 8.69 mg/g without OA, and 7.38 mg/g with OA.
185 These values were 5.5 and 3.7 times higher than those of the soaking method, respectively.
186 Besides, water-washed Zr-ACF and unwashed Zr-ACF showed the same level of fluoride
187 adsorption capacity, which indicates that the impregnated Zr(IV) did not leak into aqueous
188 solutions. Given the fact that both impregnation methods consumed the same amount of
189 chemicals, the superior fluoride adsorption capacity of drop-coating was due to more effective
190 loading of Zr(IV) onto ACF. Specifically, the drop-coating method took advantage of higher
191 Zr(IV) concentrations (because of smaller solution volume) and repeated dropwise
192 impregnations. Therefore, to achieve the same level of defluoridation performance, the drop-

193 coating method consumes much fewer chemicals and water and has a much lower PMI than the
194 soaking method.

195 Notably, the addition of OA had opposite effects on fluoride adsorption in the drop-coating
196 and the soaking methods. Zr(IV) species can interact with $-OH$ from OA to form zirconium
197 oxalate complexes. The formation of these complexes reduces the number of available binding
198 sites in Zr(IV) for attracting fluoride. This is why the adsorption capacity of Zr-ACF dropped
199 after OA was added in the drop-coating method. Moreover, the high local concentration of OA
200 could reach a supersaturation level and thus the formed complexes could precipitate and cause
201 pore blockage of Zr-ACF.

202 In the soaking method, on the contrary, the adsorption capacity of Zr-ACF had a slight
203 increase after OA was added, which is consistent with a previous study (Velazquez-Jimenez et
204 al., 2013). This is because the zirconium oxalate complexes prevented the aggregation of Zr
205 particles in the solution due to steric effects and electrostatic repulsion, thus improving the
206 distribution of Zr on the surface of ACF (Velazquez-Jimenez et al., 2013). Since the soaking
207 method had a very low Zr loading, such improvement outweighed the loss of binding sites.

208 The results revealed that the drop-coating method without OA was the best impregnation
209 method. In the following experiments, only Zr-ACF prepared by drop-coating without OA was
210 used.



211
 212 Figure 1: (A) Effect of impregnation method on fluoride adsorption capacity of Zr-ACF and (B)
 213 effect of Zr/ACF mass ratio on fluoride adsorption capacity of Zr-ACF (20 mg/L F^- , 2 g/L Zr-
 214 ACF, pH 7, 25 °C)

215 3.1.2. Different Zr/ACF mass ratios

216 As shown in Figure 1(B), the adsorption capacity of Zr-ACF increased gradually with the
 217 increase of Zr/ACF mass ratio at the beginning and then reached the highest point (9.02 mg/g)
 218 when Zr/ACF mass ratio was 0.6, which was 5.8 times higher than that of the original ACF (1.54
 219 mg/g). The amount of Zr(IV) loaded on the surface of ACF surface rose, and thus the binding
 220 sites for fluoride increased. As the Zr/ACF mass ratio increased further, the fluoride adsorption
 221 capacity declined slightly and remained relatively stable when the Zr/ACF mass ratio reached to
 222 1. The moderate decrease might be because a high concentration of Zr(IV) is unfavourable to
 223 form a uniform distribution in the channel of ACF, resulting in channel blockage (Velazquez-
 224 Jimenez et al., 2013). Although the adsorption capacity of Zr-ACF at the Zr/ACF mass ratio of 1
 225 (8.69 mg/g) was slightly higher than that at the mass ratio of 0.8 (8.61 mg/g), such minor
 226 improvement might be because the detached Zr(IV) species reacts with fluoride and forms

227 complexes in solution. Considering the trade-off between adsorption capacity and chemical
228 consumption, a moderate Zr/ACF mass ratio of 0.6 was chosen as the fixed mass ratio for further
229 study.

230 **3.2. Characterization of Zr-ACF prepared by drop-coating**

231 3.2.1. Morphology

232 The surface morphology of original ACF, Zr-ACF before and after fluoride adsorption
233 was analysed using SEM as shown in Figure S1. It can be seen that the porous surface of ACF
234 was uneven and rough which is due to the large pores of ACF. There were grooves and gaps
235 between long carbon fibres. After ACF was modified by Zr, its surface became smooth and the
236 porous structure disappeared, which is because the large pores of ACF were loaded with Zr.
237 After Zr-ACF was saturated by fluoride, the surface of Zr-ACF became even smoother,
238 suggesting that the Zr-F complexes might block the channel of Zr-ACF.

239 3.2.2. Surface area and pore size distribution

240 The summary of BET surface area and Horvath-Kawazoe pore volume is shown in Table S1.
241 After drop-coating with Zr, the BET surface area of ACF increased moderately from 1108.60 to
242 1178.96 m²/g. After adsorption of fluoride, the BET surface area of Zr-ACF decreased
243 dramatically to 768.54 m²/g. The Horvath-Kawazoe pore volume followed the same trend, which
244 increased from 0.43 to 0.46 cm³/g after ACF was modified by Zr, and then declined to 0.31
245 cm³/g after fluoride adsorption. As shown in Figure S2, the original ACF displayed a
246 monomodal pore size distribution with the peak at 0.6 nm, which indicates that ACF belongs to
247 microporous materials (Rouquerol et al., 1994). When the ACF was modified by Zr, the pore
248 size distribution became bimodal, with a larger peak at about 0.5 nm and a smaller peak at about

249 0.6 nm. After fluoride adsorption, the pore size distribution was still bimodal but the pore
250 volumes at two peaks were reduced by almost 50%, which suggests that these micropores
251 contribute most to the adsorption capacity of Zr-ACF.

252 ***3.3. Spectroscopic evidence for Zr anchoring on ACF and fluoride adsorption onto Zr-ACF***

253 ***3.3.1. FTIR analysis***

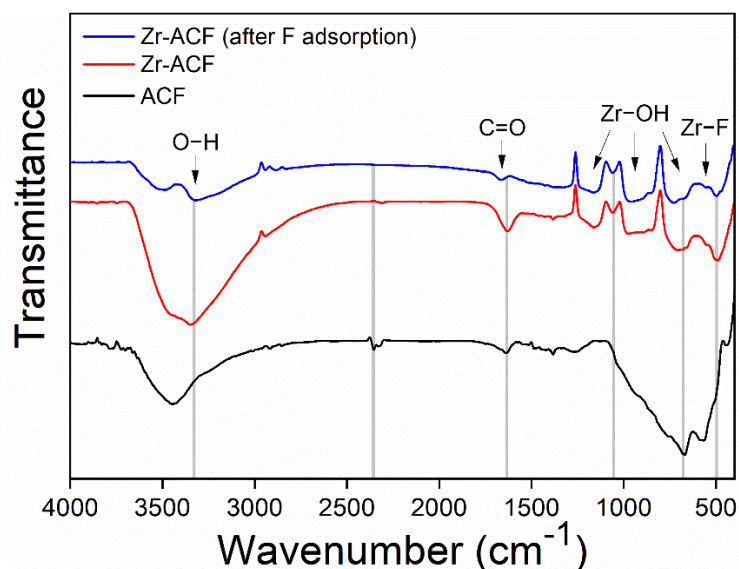
254 FTIR spectra of ACF, Zr-ACF before and after fluoride adsorption were investigated to
255 illustrate the change of surface functional groups (Figure 2). For ACF, the broad peak centred at
256 3441 cm^{-1} is due to stretching of -OH groups in adsorbed water (Yu et al., 2018). The peak at
257 1635 cm^{-1} is the stretching of C=O bonds of -COOH groups. The peaks at 2331 and 2350 cm^{-1}
258 are due to the presence of atmospheric CO_2 on the ACF surface.

259 For Zr-ACF, the broad -OH peak was blue-shifted due to the formation of Zr-OH groups
260 (Bollino et al., 2017). The C=O bonds had a slight shift because Zr(IV) species interacts with
261 -COOH groups through electrostatic interactions to form C-O-Zr bonds (Velazquez-Jimenez et
262 al., 2013). The peak at 1160 cm^{-1} is due to the combined effects of Zr-OH and C-O groups, as
263 the double bond in -COOH group breaks down and forms new bonds with Zr(IV) . The peaks at
264 1060 cm^{-1} may be associated with the vibration of Zr=O bonds (Mullick and Neogi, 2018). The
265 broad peaks between 980 and 845 cm^{-1} represent a combination of Zr-O and Zr-OH bonds
266 (Velazquez-Jimenez, 2014). The peaks between 718 and 660 cm^{-1} are due to the bending of
267 Zr-OH bonds, formed from combining with -OH groups on ACF surface (Yakout and Hassan,
268 2014). The small peaks at 491 cm^{-1} can also be attributed to Zr-O bonds (Vitanov et al., 2014).

269 For Zr-ACF after fluoride adsorption, the -OH peak had a lower intensity than that before
270 fluoride adsorption, which indicates that -OH groups played a role in the fluoride adsorption

271 process. The C=O peak was further shifted to 1670 cm^{-1} due to the interaction between Zr on the
272 C–O–Zr bond and F^- . The broad peaks between 980 and 845 cm^{-1} are of a greater intensity
273 compared to that before fluoride adsorption which may suggest additional absorption by Zr–O
274 bonds in ZrOF_2 formations (Gong et al., 2012). Small peaks between 600 and 524 cm^{-1} may be
275 due to stretching of Zr–F bonds (Gong et al., 2012).

276



277

278 Figure 2: FTIR spectra of original ACF, Zr-ACF before and after fluoride adsorption

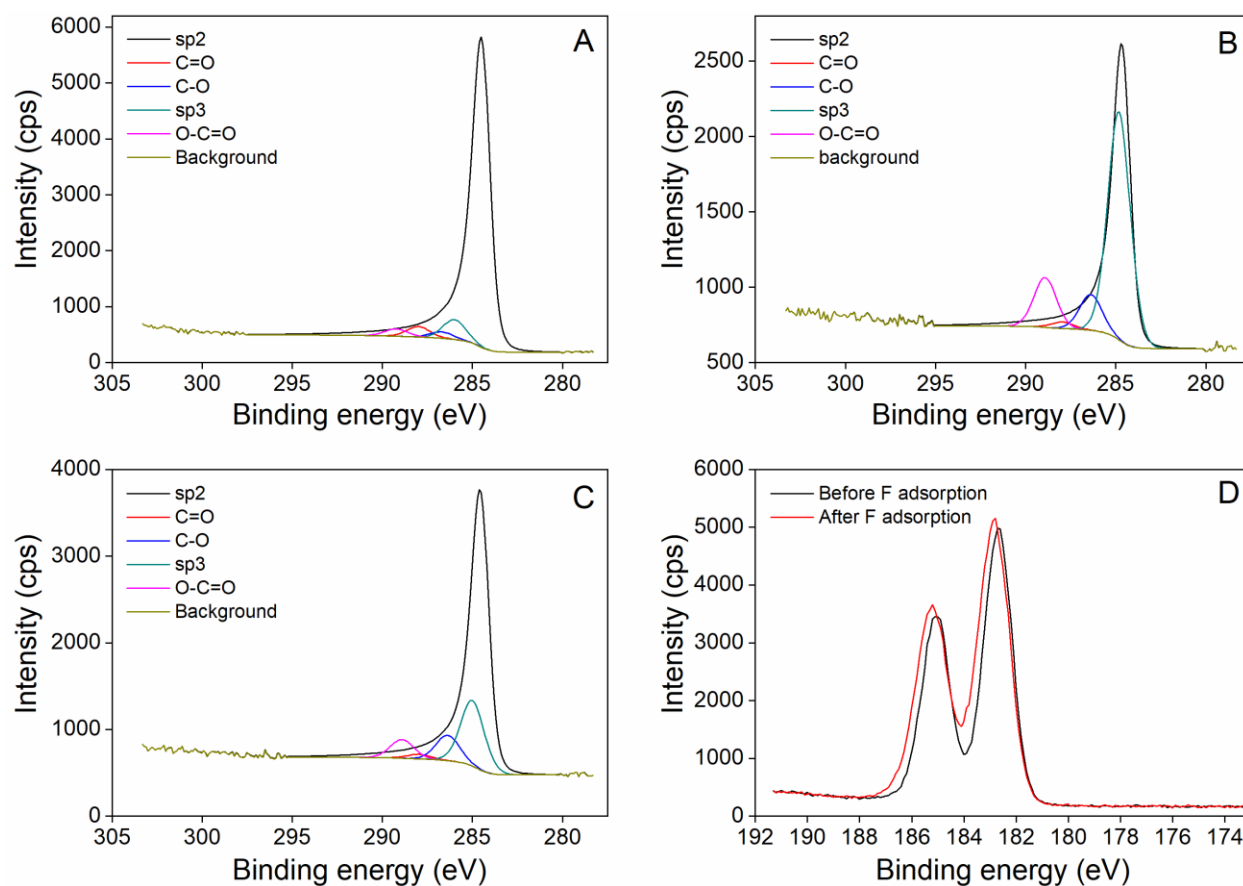
279 3.3.2. XPS analysis

280 XPS analysis was conducted to seek out the probable Zr(IV) structure formed during the
281 drop-coating process and the way that fluoride interacts with the metal complex. XPS spectra in
282 the C 1s region are demonstrated in Figure 3(A), (B) and (C) representing original ACF, Zr-ACF
283 before and after fluoride adsorption, respectively. For all the three samples, the highest intensity
284 peak is at 284.6 eV, which is attributed to sp^2 C=C bonds. The broad asymmetric tail towards

285 increasing binding energy indicates a high concentration of sp^2 carbon in the samples. All
286 samples showed peaks for C=O and O–C=O bonds at 287.9 eV and 288.9 eV, respectively.

287 From ACF to Zr-ACF, the peak associated with sp^3 carbon bonding was shifted from 286.0
288 to 284.9 eV and was at a higher intensity, suggesting that carbon atoms on the surface of ACF
289 undergo sp^3 hybridisation to form bonds with Zr(IV). Modifying the surface with the less
290 electronegative element Zr increases the electronic density around the base element and decreases
291 the binding energy (Tardio and Cumpson, 2018). After Zr-ACF was saturated by fluoride, the
292 intensity of the O–C=O peak at 288.9 eV declined noticeably. Such change is due to the
293 interaction between Zr on the C–O–Zr bond and F, which was also revealed by the FTIR spectra.

294 Figure 3(D) shows the XPS spectra in the Zr 3d region corrected to C 1s region. The
295 doublet peaks at 182.7 eV and 185.1 eV correspond to Zr–OH bonds in Zr 3d_{5/2} and Zr 3d_{3/2}
296 regions, respectively (Gondal et al., 2018). Both the peaks were shifted by 0.1 eV towards higher
297 binding energies after fluoride adsorption. The shift indicates the formation of Zr–F bonds
298 because F is the most electronegative element and thus the binding energy of Zr–F is higher than
299 that of Zr–OH bond (Velazquez-Jimenez et al., 2013). The FTIR and XPS analysis identified the
300 main functional groups involved in both the anchoring of Zr(IV) on ACF and the adsorption of
301 fluoride onto Zr-ACF.



302
 303 Figure 3: XPS spectra in the C 1s region for (A) ACF, (B) Zr-ACF, (C) Zr-ACF after fluoride
 304 adsorption, (D) the Zr 3d region for Zr-ACF before and after fluoride adsorption

305 3.4. Adsorption mechanisms at different pH levels

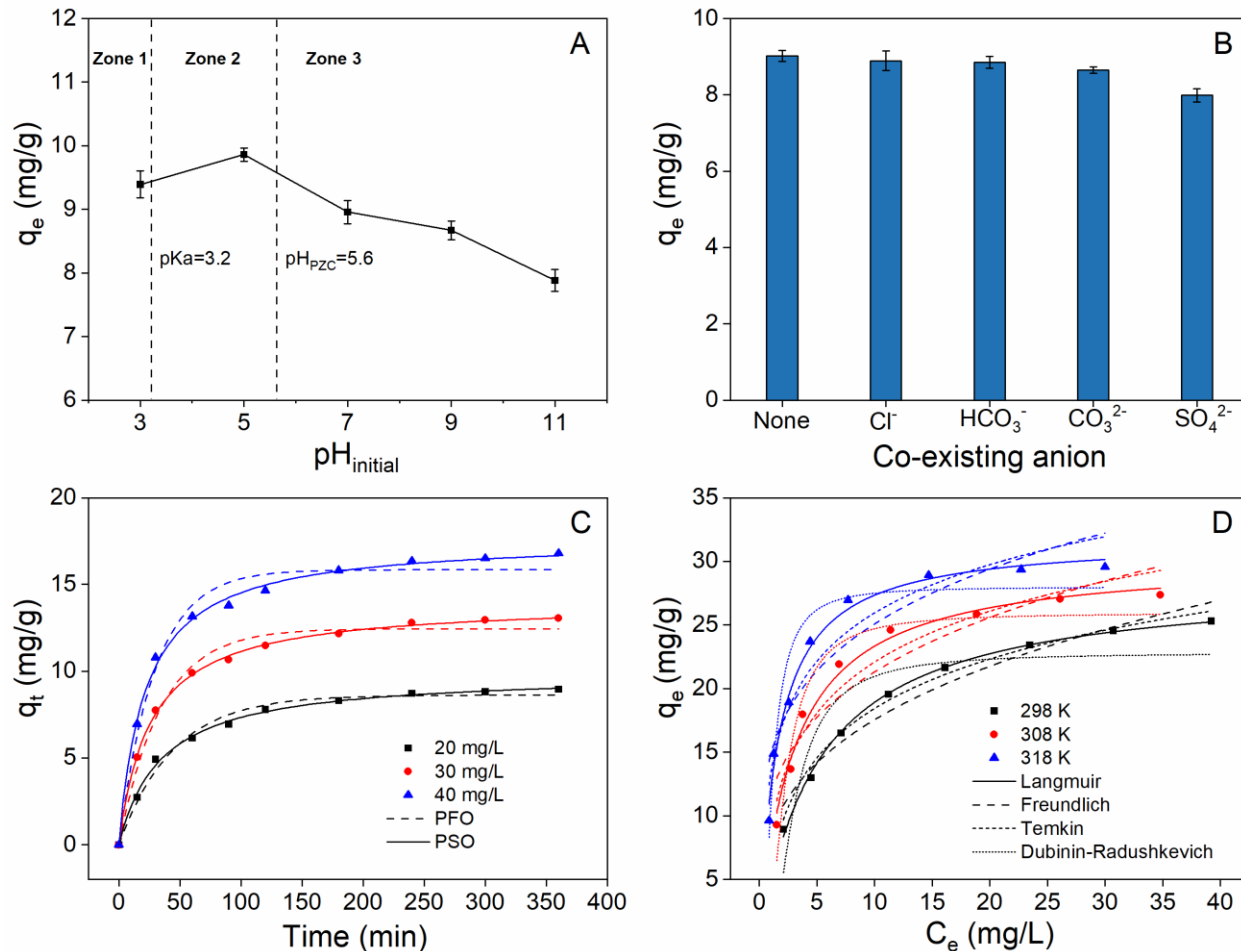
306 The initial pH of the solution plays a critical role in the adsorption process because it
 307 changes the surface charge properties of both adsorbent and adsorbate (Sairam Sundaram et al.,
 308 2008). As a result, various adsorption mechanisms will occur and affect adsorption behaviours at
 309 different pH levels. The surface charge of Zr-ACF was characterized by pH_{PZC} which was found
 310 to be 5.6 (Figure S3). The speciation of fluoride was characterized by the acid dissociation
 311 constant pK_a which is 3.2 (Figure S4). Hence the entire pH range of 3-11 can be distinctly
 312 divided into three zones by pH_{PZC} and pK_a (Figure 4(A)): in Zone 1 ($pH < 3.2$), Zr-ACF is

313 positively charged while more than 50% of F species exists as hydrofluoric acid (HF) with no
314 charge; in Zone 2 ($3.2 < \text{pH} < 5.6$), Zr-ACF is still positively charged whereas the majority of F
315 species becomes F^- ; in Zone 3 ($\text{pH} > 5.6$), Zr-ACF becomes negatively charged and F^- is also
316 negatively charged.

317 As illustrated in Figure 4(A), q_e increased moderately from Zone 1 to Zone 2 and
318 decreased substantially from Zone 2 to Zone 3. For the experiment in Zone 1, the solution pH
319 increased after fluoride adsorption (Table S2), indicating that fluoride adsorption onto Zr-ACF is
320 primarily the result of ion exchange between F^- and OH^- . As discussed in Section 3.3, the
321 surfaces of Zr-ACF are covered with $-\text{OH}$ groups. In the ion exchange process, these $-\text{OH}$
322 groups are replaced by F^- , and new Zr-F covalent bonds are formed between Zr(IV) species
323 (Lewis acid) and F^- (Lewis base) (Wu et al., 2020). The electrostatic attraction between Zr-ACF
324 and partially dissociated F^- may also account for the adsorption.

325 For the experiment in Zone 2, the pH had a smaller increase after fluoride adsorption
326 (Table S2), which means ion exchange still contributes to the adsorption process but to a lesser
327 extent. Instead, the strong electrostatic attraction between Zr-ACF and fully dissociated F^-
328 becomes the principal adsorption mechanism. The maximum q_e of 9.85 mg/g was observed at
329 pH 5 because pH 5 was the nearest to the pH_{PZC} of 5.6.

330 For the experiments in Zone 3, the final pH values were always lower than the initial
331 values (Table S2). This indicates that excessive OH^- in the solution competes with F^- for binding
332 sites on Zr-ACF, which is not beneficial for the ion exchange process. Furthermore, electrostatic
333 forces between Zr-ACF and F^- change from electrostatic attraction to electrostatic repulsion.
334 Therefore, q_e decreased dramatically from Zone 2 to Zone 3.



335
 336 Figure 4: (A) Effect of initial pH on the adsorption capacity of Zr-ACF (20 mg/L F^- , 2 g/L Zr-
 337 ACF, 25 °C); (B) effect of co-existing anions on fluoride adsorption capacity (20 mg/L F^- , 2 g/L
 338 Zr-ACF, pH 7, 25 °C); (C) adsorption kinetics of fluoride onto Zr-ACF at different fluoride
 339 concentrations (2 g/L Zr-ACF, pH 7, 25 °C); (D) adsorption isotherms of fluoride onto Zr-ACF
 340 at different temperatures (2 g/L Zr-ACF, pH 7)

341 3.5. Effect of co-existing anions

342 Natural waters contain various anions which may interfere with the fluoride adsorption
 343 process. As shown in Figure 4(B), the uptake of fluoride by Zr-ACF was affected by co-existing
 344 anions in the following order: $SO_4^{2-} > CO_3^{2-} > HCO_3^- > Cl^-$. Three anions (Cl^- , HCO_3^- and

345 CO_3^{2-}) had an insignificant negative impact on q_e , which decreased by 1.5%, 1.9% and 4.2%,
346 respectively. It should be noted that some researchers reported that HCO_3^- inhibited the
347 adsorption of fluoride because it had a buffering effect on the solution pH (Kumar et al., 2009;
348 Shen et al., 2018).

349 By contrast, q_e decreased by 11.5% in the presence of SO_4^{2-} . This is perhaps because
350 SO_4^{2-} has more negative charges and is a stronger Lewis base than F^- (Daifullah et al., 2007); so
351 it can be more strongly attracted to Lewis acid sites on Zr-ACF surface. Moreover, F^- and SO_4^{2-}
352 tend to form inner-sphere complexes with binding surfaces, while other anions such as Cl^- and
353 CO_3^{2-} generally form outer-sphere complexes (Kumar et al., 2011; Wu et al., 2020). Inner-sphere
354 complexation involves a much stronger interaction than outer-sphere complexation. This
355 provides a strong driving force to adsorb F^- from other anions except for SO_4^{2-} .

356 **3.6. Adsorption kinetics, isotherms, and thermodynamics**

357 Adsorption kinetics identify the required equilibrium time for an adsorption process (Tran
358 et al., 2017). As shown in Figure 4(C), fluoride adsorption by Zr-ACF was most rapid in the first
359 30 minutes with more than 50% of the initial fluoride concentration were removed. Such rapid
360 adsorption rate is due to the initial steep concentration gradient between the solution and the
361 surface of Zr-ACF as well as the large number of vacant pores (Zhang et al., 2018). The
362 adsorption rate then decreased gradually until the equilibrium was reached after 360 min. The
363 kinetics data were fitted to the pseudo-first-order (PFO) and the pseudo-second-order (PSO)
364 models (Figure 4(C)). The equations of the models are provided in the Supplementary
365 Information. The kinetic parameters, together with the standard deviation SD and the coefficient
366 of determination R^2 , are listed in Table S3. It can be seen that the PSO model had a higher R^2

367 (>0.995) and a lower SD than the PFO model under all three fluoride concentrations. Therefore,
368 the PSO model is more suitable for the description of the adsorption kinetics of fluoride onto Zr-
369 ACF. These results are consistent with the adsorption of fluoride onto other adsorbents, such as
370 activated carbon and aluminium hydroxide (Gai et al., 2015; Mullick and Neogi, 2018).

371 Adsorption isotherms describe the equilibrium relationship between the adsorbate and the
372 adsorbent (Tran et al., 2017; Dehghani et al., 2018). As shown in Figure 4(D), the adsorption
373 capacity of Zr-ACF at equilibrium increased with the increasing temperature, which indicates the
374 endothermic nature of the adsorption process. The experimental data were fitted to four widely
375 used isotherm models, namely the Langmuir, Freundlich, Temkin and Dubinin-Radushkevich
376 (D-R) models. The descriptions of the four models, including their nonlinear equations, are
377 included in the Supplementary Information. The fitting curves of the four models are shown in
378 Figure 4(D) and the isotherms parameters and the coefficient of determination R^2 are given in
379 Table S4. Among the four models, the Langmuir model was found to be best fitted to the
380 experimental data as the R^2 values of the Langmuir model (varied from 0.985 to 0.997) are
381 invariably higher than those of other models at every temperature. This suggests that the fluoride
382 adsorption process is monolayer molecular adsorption and it occurs homogeneously on the
383 surface of Zr-ACF (Langmuir, 1918). The separation factor (R_L) of the Langmuir model, which
384 indicates the favourability of the adsorption process, was calculated and shown in Figure S5. The
385 value of R_L can be either irreversible ($R_L = 0$), favourable ($0 < R_L < 1$), linear ($R_L = 1$), or
386 unfavourable ($R_L > 1$) (Weber and Chakravorti, 1974). The R_L values at all three temperatures
387 were always below 0.25, indicating that the adsorption process was extremely favourable.

388 Table S5 compares the Langmuir maximum adsorption capacity (q_m) of various carbon-
389 based adsorbents for fluoride removal. The q_m of Zr-ACF prepared in this study was 28.50 mg/g

390 when the adsorbent dose was 2 g/L, the pH was 7 and the temperature was 25 °C. Apparently,
391 Zr-ACF exhibits superior performance over other carbon-based adsorbents reported in the
392 literature.

393 Adsorption thermodynamics indicate the feasibility of the adsorption processes. The
394 values of the thermodynamic parameters are shown in Table S6. The negative values of ΔG° at
395 all three temperatures denote the spontaneity of the adsorption process (Li et al., 2005; Khan et
396 al., 2020). As the temperature rose, the absolute value of ΔG° increased implying that the
397 adsorption process is more favourable at a higher temperature. The positive values of ΔH°
398 confirm that the adsorption process is endothermic (Gao et al., 2013). The positive values of ΔS°
399 imply increasing randomness of the process (Ghaedi et al., 2012). In summary, the adsorption
400 process of fluoride onto Zr-ACF is spontaneous and endothermic.

401

402 **4. Conclusion**

403 In this study, we have presented a new drop-coating method to prepare Zr-ACF
404 adsorbents for fluoride removal. Compared to the traditional soaking method, the drop-coating
405 method achieved a 5.5 times higher fluoride adsorption capacity while consumed much fewer
406 chemicals and no complexing agents. The optimal Zr/ACF mass ratio for fluoride removal was
407 0.6. SEM and BET results showed that Zr-ACF prepared by drop-coating had smoother surface
408 and greater surface area than the original ACF. The micropores contribute most to the adsorption
409 capacity of Zr-ACF. FTIR and XPS results showed that -OH groups played a key role in the
410 anchoring of Zr(IV) on ACF and the adsorption of fluoride onto Zr-ACF. Ion exchange and
411 electrostatic attraction were the two main adsorption mechanisms and they dominated in

412 different pH zones that were divided by pH_{PZC} of Zr-ACF and pK_a of fluoride. Various co-
413 existing anions, except for SO_4^{2-} , had insignificant influence on the fluoride adsorption capacity
414 of Zr-ACF. The PSO model was suitable in describing the adsorption kinetics and the Langmuir
415 model was best fit to the isotherms data with the maximum adsorption capacity obtained at 25 °C
416 up to 28.50 mg/L. The thermodynamic study revealed that the adsorption process was
417 spontaneous and endothermic in nature.

418 The results have demonstrated that Zr-ACF produced by drop-coating is an efficient and
419 cost-effective adsorbent for fluoride removal due to its ease of synthesis, reduced chemical
420 consumption and improved adsorption capacity. The drop-coating method can be easily scaled
421 up by using commercial sprayers, which makes it highly practical in rural and remote areas of
422 developing countries. However, further research is needed to assess the environmental impact of
423 Zr-ACF and develop an appropriate recycling strategy before it can be used for large-scale
424 applications.

425 **Acknowledgements**

426 This research was supported by the Royal Academy of Engineering under the Research
427 Fellowship scheme (RF_201718_17145). XPS data collection was performed at the EPSRC
428 National Facility for XPS ('HarwellXPS'), operated by Cardiff University and UCL, under
429 contract No. PR16195.

430 **References**

431 Akuno, M.H., Nocella, G., Milia, E.P., Gutierrez, L., 2019. Factors influencing the relationship
432 between fluoride in drinking water and dental fluorosis: a ten-year systematic review and meta-
433 analysis. *Journal of Water and Health*.

- 434 Ali, S., Fakhri, Y., Golbini, M., Thakur, S.K., Alinejad, A., Parseh, I., Shekhar, S., Bhattacharya,
435 P., 2019. Concentration of fluoride in groundwater of India: A systematic review, meta-analysis
436 and risk assessment. *Groundwater for Sustainable Development*, 100224.
- 437 Ali, S., Thakur, S.K., Sarkar, A., Shekhar, S., 2016. Worldwide contamination of water by
438 fluoride. *Environmental Chemistry Letters* 14, 291-315.
- 439 Amini, H., Haghghat, G.A., Yunesian, M., Nabizadeh, R., Mahvi, A.H., Dehghani, M.H.,
440 Davani, R., Aminian, A.-R., Shamsipour, M., Hassanzadeh, N., 2016. Spatial and temporal
441 variability of fluoride concentrations in groundwater resources of Larestan and Gerash regions in
442 Iran from 2003 to 2010. *Environmental Geochemistry and Health* 38, 25-37.
- 443 Ansari, M., Kazemipour, M., Dehghani, M., Kazemipour, M., 2011. The defluoridation of
444 drinking water using multi-walled carbon nanotubes. *Journal of Fluorine Chemistry* 132, 516-
445 520.
- 446 Bhaumik, R., Mondal, N.K., 2015. Adsorption of fluoride from aqueous solution by a new low-
447 cost adsorbent: thermally and chemically activated coconut fibre dust. *Clean Technologies and*
448 *Environmental Policy* 17, 2157-2172.
- 449 Bollino, F., Armenia, E., Tranquillo, E., 2017. Zirconia/hydroxyapatite composites synthesized
450 via Sol-Gel: Influence of hydroxyapatite content and heating on their biological properties.
451 *Materials* 10, 757.
- 452 Crnosija, N., Choi, M., Meliker, J.R., 2019. Fluoridation and county-level secondary bone cancer
453 among cancer patients 18 years or older in New York State. *Environmental Geochemistry and*
454 *Health* 41, 761-768.
- 455 Daifullah, A., Yakout, S., Elreefy, S., 2007. Adsorption of fluoride in aqueous solutions using
456 KMnO₄-modified activated carbon derived from steam pyrolysis of rice straw. *Journal of*
457 *Hazardous materials* 147, 633-643.
- 458 Dehghani, M.H., Faraji, M., Mohammadi, A., Kamani, H., 2017. Optimization of fluoride
459 adsorption onto natural and modified pumice using response surface methodology: isotherm,
460 kinetic and thermodynamic studies. *Korean Journal of Chemical Engineering* 34, 454-462.
- 461 Dehghani, M.H., Zarei, A., Mesdaghinia, A., Nabizadeh, R., Alimohammadi, M., Afsharnia, M.,
462 McKay, G., 2018. Production and application of a treated bentonite–chitosan composite for the
463 efficient removal of humic acid from aqueous solution. *Chemical Engineering Research and*
464 *Design* 140, 102-115.
- 465 Dehghani, M.H., Zarei, A., Yousefi, M., Asghari, F.B., Haghghat, G.A., 2019. Fluoride
466 contamination in groundwater resources in the southern Iran and its related human health risks.
467 *Desalination and Water Treatment* 153, 95-104.
- 468 Fawell, J., Bailey, K., Chilton, J., Dahi, E., Magara, Y., 2006. Fluoride in drinking-water. IWA
469 publishing.

- 470 Gai, W.-Z., Deng, Z.-Y., Shi, Y., 2015. Fluoride removal from water using high-activity
471 aluminum hydroxide prepared by the ultrasonic method. *RSC Advances* 5, 84223-84231.
- 472 Gan, Y., Wang, X., Zhang, L., Wu, B., Zhang, G., Zhang, S., 2019. Coagulation removal of
473 fluoride by zirconium tetrachloride: Performance evaluation and mechanism analysis.
474 *Chemosphere* 218, 860-868.
- 475 Gao, H., Kan, T., Zhao, S., Qian, Y., Cheng, X., Wu, W., Wang, X., Zheng, L., 2013. Removal
476 of anionic azo dyes from aqueous solution by functional ionic liquid cross-linked polymer.
477 *Journal of Hazardous materials* 261, 83-90.
- 478 García-Sánchez, J., Solache-Ríos, M., Martínez-Gutiérrez, J., Arteaga-Larios, N., Ojeda-
479 Escamilla, M., Rodríguez-Torres, I., 2016. Modified natural magnetite with Al and La ions for
480 the adsorption of fluoride ions from aqueous solutions. *Journal of Fluorine Chemistry* 186, 115-
481 124.
- 482 Ghaedi, M., Sadeghian, B., Pebdani, A.A., Sahraei, R., Daneshfar, A., Duran, C., 2012. Kinetics,
483 thermodynamics and equilibrium evaluation of direct yellow 12 removal by adsorption onto
484 silver nanoparticles loaded activated carbon. *Chemical Engineering Journal* 187, 133-141.
- 485 Gondal, M.A., Fasasi, T.A., Baig, U., Mekki, A., 2018. Effects of oxidizing media on the
486 composition, morphology and optical properties of colloidal zirconium oxide nanoparticles
487 synthesized via pulsed laser ablation in liquid technique. *Journal of Nanoscience and*
488 *Nanotechnology* 18, 4030-4039.
- 489 Gong, Y., Andrews, L., Bauschlicher, C.W., Thanthiriwatte, K.S., Dixon, D., 2012. Infrared
490 spectroscopic and theoretical studies of the OTiF₂, OZrF₂ and OHfF₂ molecules with terminal
491 oxo ligands. *Dalton Trans.* 41, 11706-11715.
- 492 Górski, Ł., Saniewska, A., Parzuchowski, P., Meyerhoff, M.E., Malinowska, E., 2005.
493 Zirconium(IV)-salophens as fluoride-selective ionophores in polymeric membrane electrodes.
494 *Analytica Chimica Acta* 551, 37-44.
- 495 Green, R., Lanphear, B., Hornung, R., Flora, D., Martinez-Mier, E.A., Neufeld, R., Ayotte, P.,
496 Muckle, G., Till, C., 2019. Association between maternal fluoride exposure during pregnancy
497 and IQ scores in offspring in Canada. *JAMA Pediatrics* 173, 940-948.
- 498 Grzegorzek, M., Majewska-Nowak, K., 2016. Use of the electrodialysis process for fluoride ion
499 and salt removal from multi-constituent aqueous solutions. *Architecture Civil Engineering*
500 *Environment* 9, 107--113.
- 501 Halvorson, R.A., Leng, W., Vikesland, P.J., 2011. Differentiation of microcystin, nodularin, and
502 their component amino acids by drop-coating deposition Raman spectroscopy. *Analytical*
503 *Chemistry* 83, 9273-9280.

- 504 He, Z., Lan, H., Gong, W., Liu, R., Gao, Y., Liu, H., Qu, J., 2016. Coagulation behaviors of
505 aluminum salts towards fluoride: significance of aluminum speciation and transformation.
506 Separation and Purification Technology 165, 137-144.
- 507 Kalidindi, S., Vecha, M., Kar, A., Raychoudhury, T., 2016. Aluminum–cerium double-metal
508 impregnated activated carbon: a novel composite for fluoride removal from aqueous solution.
509 Water Supply 17, 115-124.
- 510 Khan, Z.H., Gao, M., Qiu, W., Islam, M.S., Song, Z., 2020. Mechanisms for cadmium adsorption
511 by magnetic biochar composites in an aqueous solution. Chemosphere 246, 125701.
- 512 Kumar, E., Bhatnagar, A., Ji, M., Jung, W., Lee, S.-H., Kim, S.-J., Lee, G., Song, H., Choi, J.-Y.,
513 Yang, J.-S., Jeon, B.-H., 2009. Defluoridation from aqueous solutions by granular ferric
514 hydroxide (GFH). Water Research 43, 490-498.
- 515 Kumar, E., Bhatnagar, A., Kumar, U., Sillanpää, M., 2011. Defluoridation from aqueous
516 solutions by nano-alumina: Characterization and sorption studies. Journal of Hazardous materials
517 186, 1042-1049.
- 518 Langmuir, I., 1918. The adsorption of gases on plane surfaces of glass, mica and platinum.
519 Journal of the American Chemical Society 40, 1361-1403.
- 520 Li, Y.-H., Di, Z., Ding, J., Wu, D., Luan, Z., Zhu, Y., 2005. Adsorption thermodynamic, kinetic
521 and desorption studies of Pb²⁺ on carbon nanotubes. Water Research 39, 605-609.
- 522 Li, Y., 2011. Surface modification technique for acoustic chemical sensor arrays based on
523 CMUTs.
- 524 Li, Y., Zhang, C., Jiang, Y., Wang, T.-J., 2018. Electrically enhanced adsorption and green
525 regeneration for fluoride removal using Ti(OH)₄-loaded activated carbon electrodes.
526 Chemosphere 200, 554-560.
- 527 Lu, N.C., Liu, J., 2010. Removal of phosphate and fluoride from wastewater by a hybrid
528 precipitation–microfiltration process. Separation and Purification Technology 74, 329-335.
- 529 Malago, J., Makoba, E., Muzuka, A.N., 2017. Fluoride levels in surface and groundwater in
530 Africa: A review. American Journal of Water Science and Engineering 3, 1-17.
- 531 Mukherjee, I., Singh, U.K., 2018. Groundwater fluoride contamination, probable release, and
532 containment mechanisms: a review on Indian context. Environmental Geochemistry and Health
533 40, 2259-2301.
- 534 Mullick, A., Neogi, S., 2018. Acoustic cavitation induced synthesis of zirconium impregnated
535 activated carbon for effective fluoride scavenging from water by adsorption. Ultrasonics
536 Sonochemistry 45, 65-77.

- 537 Nie, Y., Hu, C., Kong, C., 2012. Enhanced fluoride adsorption using Al (III) modified calcium
538 hydroxyapatite. *Journal of Hazardous materials* 233, 194-199.
- 539 Owusu-Agyeman, I., Reinwald, M., Jeihanipour, A., Schäfer, A.I., 2019. Removal of fluoride
540 and natural organic matter from natural tropical brackish waters by nanofiltration/reverse
541 osmosis with varying water chemistry. *Chemosphere* 217, 47-58.
- 542 Petersen, P.E., Ogawa, H., 2016. Prevention of dental caries through the use of fluoride—the
543 WHO approach. *Community Dent Health* 33, 66-68.
- 544 Rouquerol, J., Avnir, D., Fairbridge, C.W., Everett, D.H., Haynes, J.M., Pernicone, N., Ramsay,
545 J.D.F., Sing, K.S.W., Unger, K.K., 1994. Recommendations for the characterization of porous
546 solids (Technical Report). *Pure and Applied Chemistry* 66, 1739-1758.
- 547 Saha, D., Grappe, H.A., 2017. 5 - Adsorption properties of activated carbon fibers. in: Chen, J.Y.
548 (Ed.). *Activated Carbon Fiber and Textiles*. Woodhead Publishing, Oxford, pp. 143-165.
- 549 Sairam Sundaram, C., Viswanathan, N., Meenakshi, S., 2008. Defluoridation chemistry of
550 synthetic hydroxyapatite at nano scale: Equilibrium and kinetic studies. *Journal of Hazardous*
551 *materials* 155, 206-215.
- 552 Shen, J., Evangelista, M.F., Mkongo, G., Wen, H., Langford, R., Rosair, G., McCoustra, M.R.S.,
553 Arrighi, V., 2018. Efficient defluoridation of water by Monetite nanorods. *Adsorption* 24, 135-
554 145.
- 555 Shen, J., Schäfer, A.I., 2015. Factors affecting fluoride and natural organic matter (NOM)
556 removal from natural waters in Tanzania by nanofiltration/reverse osmosis. *Science of the Total*
557 *Environment* 527–528, 520-529.
- 558 Sundaram, C.S., Meenakshi, S., 2009. Fluoride sorption using organic–inorganic hybrid type ion
559 exchangers. *Journal of Colloid and Interface Science* 333, 58-62.
- 560 Talat, M., Mohan, S., Dixit, V., Singh, D.K., Hasan, S.H., Srivastava, O.N., 2018. Effective
561 removal of fluoride from water by coconut husk activated carbon in fixed bed column:
562 Experimental and breakthrough curves analysis. *Groundwater for Sustainable Development* 7,
563 48-55.
- 564 Tardio, S., Cumpson, P.J., 2018. Practical estimation of XPS binding energies using widely
565 available quantum chemistry software. *Surface and Interface Analysis* 50, 5-12.
- 566 Tran, H.N., You, S.-J., Hosseini-Bandegharai, A., Chao, H.-P., 2017. Mistakes and
567 inconsistencies regarding adsorption of contaminants from aqueous solutions: A critical review.
568 *Water Research* 120, 88-116.
- 569 Velazquez-Jimenez, L.H., 2014. Zirconium–Carbon Hybrid Sorbent for Removal of Fluoride
570 from Water: Oxalic Acid Mediated Zr(IV) Assembly and Adsorption Mechanism.
571 *Environmental Science & Technology* 48, 1166-1175.

- 572 Velazquez-Jimenez, L.H., Hurt, R.H., Matos, J., Rangel-Mendez, J.R., 2013. Zirconium–carbon
573 hybrid sorbent for removal of fluoride from water: oxalic acid mediated Zr (IV) assembly and
574 adsorption mechanism. *Environmental Science & Technology* 48, 1166-1174.
- 575 Vences-Alvarez, E., Velazquez-Jimenez, L.H., Chazaro-Ruiz, L.F., Diaz-Flores, P.E., Rangel-
576 Mendez, J.R., 2015. Fluoride removal in water by a hybrid adsorbent lanthanum–carbon. *Journal*
577 *of Colloid and Interface Science* 455, 194-202.
- 578 Vitanov, P., Harizanova, A., Ivanova, T., 2014. Characterization of ZrO₂ and (ZrO₂)_x(Al₂O₃)_{1-x}
579 thin films on Si substrates: effect of the Al₂O₃ component. *Journal of Physics: Conference Series*
580 514, 012011.
- 581 Wang, B.-y., Chen, Z.-l., Zhu, J., Shen, J.-m., Han, Y., 2013. Pilot-scale fluoride-containing
582 wastewater treatment by the ballasted flocculation process. *Water Science and Technology* 68,
583 134-143.
- 584 Wang, M., Li, X., He, W.-y., Li, J.-x., Zhu, Y.-y., Liao, Y.-L., Yang, J.-y., Yang, X.-e., 2019.
585 Distribution, health risk assessment, and anthropogenic sources of fluoride in farmland soils in
586 phosphate industrial area, southwest China. *Environmental Pollution* 249, 423-433.
- 587 Wang, Y., Chen, N., Wei, W., Cui, J., Wei, Z., 2011. Enhanced adsorption of fluoride from
588 aqueous solution onto nanosized hydroxyapatite by low-molecular-weight organic acids.
589 *Desalination* 276, 161-168.
- 590 Weber, T.W., Chakravorti, R.K., 1974. Pore and solid diffusion models for fixed-bed adsorbers.
591 *AIChE Journal* 20, 228-238.
- 592 Welton, T., 2015. Solvents and sustainable chemistry. *Proceedings of the Royal Society A:*
593 *Mathematical, Physical and Engineering Sciences* 471, 20150502.
- 594 World Health Organization, 2017. Guidelines for drinking-water quality, 4th edition,
595 incorporating the 1st addendum. Switzerland.
- 596 Wu, B., Wan, J., Zhang, Y., Pan, B., Lo, I.M.C., 2020. Selective phosphate removal from water
597 and wastewater using sorption: Process fundamentals and removal mechanisms. *Environmental*
598 *Science & Technology* 54, 50-66.
- 599 Yakout, S.M., Hassan, H.S., 2014. Adsorption characteristics of sol gel-derived zirconia for
600 cesium ions from aqueous solutions. *Molecules (Basel, Switzerland)* 19, 9160.
- 601 Yousefi, M., Ghalehaskar, S., Asghari, F.B., Ghaderpoury, A., Dehghani, M.H., Ghaderpoori, M.,
602 Mohammadi, A.A., 2019. Distribution of fluoride contamination in drinking water resources and
603 health risk assessment using geographic information system, northwest Iran. *Regulatory*
604 *Toxicology and Pharmacology* 107, 104408.

- 605 Yu, Z., Xu, C., Yuan, K., Gan, X., Feng, C., Wang, X., Zhu, L., Zhang, G., Xu, D., 2018.
606 Characterization and adsorption mechanism of ZrO₂ mesoporous fibers for health-hazardous
607 fluoride removal. *Journal of Hazardous materials* 346, 82-92.
- 608 Zhang, L., Zhao, L., Zeng, Q., Fu, G., Feng, B., Lin, X., Liu, Z., Wang, Y., Hou, C., 2020.
609 Spatial distribution of fluoride in drinking water and health risk assessment of children in typical
610 fluorosis areas in north China. *Chemosphere* 239, 124811.
- 611 Zhang, Z., Li, Y., Chen, H., Zhang, X., Li, H., 2018. The systematic adsorption of diclofenac
612 onto waste red bricks functionalized with iron oxides. *Water* 10, 1343.
613